CrystEngComm

Accepted Manuscript

ROYAL SOCIETY OF CHEMISTRY

www.rsc.org/crystengcomm

Cite this: DOI: 10.1039/c0xx00000x

www.rsc.org/xxxxxx

ARTICLE TYPE

Growth Mechanism of Vertically Aligned SnSe Nanosheets via Physical Vapour Deposition

Xing-Hua Ma,‡ Ki-Hyun Cho‡ and Yun-Mo Sung*

Received (in XXX, XXX) Xth XXXXXXXXX 20XX, Accepted Xth XXXXXXXXX 20XX

DOI: 10.1039/b000000x

Vertically aligned SnSe nanosheets were successfully synthesized on different substrates (silicon, quartz, and fluorine-doped tin oxide glass) via a non-catalytic vapour phase synthesis method for the first time. Such substrate independent feature could benefit the fabrication and application of various nanodevices due to the considerably enhanced surface area. The SnSe nanosheets have the thickness of ~ 20−30 nm and the lateral dimension of several micrometers. The analyses using X-ray diffraction and high-resolution transmission electron microscopy demonstrate that the nanosheets are single crystalline with an orthorhombic crystal structure of the Pnma 62 space group. Two-dimensional nanosheets were formed due to the anisotropic atomic bonding nature of the SnSe crystal, which is apparently different from the oriented attachment growth or the exposed plane suppressing growth. They also revealed faceted edge planes, which was elucidated in detail based upon the difference in the surface energy of each atomic plane. SnSe nanosheets show a direct band gap of ~1.1 eV, ideally meeting the requirements as high-performance light absorbing materials for solar cell applications.

Introduction

Since graphene has been proved to have many intriguing properties and great potential for various applications,[1-6] two-dimensional (2D) inorganic nanomaterials such as, hexagonal boron nitride (h-BN),[7] transition-metal dichalcogenides (MoS_2, WS_2, $NbSe_2$ and $NiTe_2$, etc.),[8] transition metal oxides (SnO_2, TiO_2, etc.),[9] etc. have also attracted renewed and unprecedented interests. In the past few years, theoretical or experimental research work has demonstrated that these 2D nanomaterials could exhibit unique properties compared to the widely studied zero-dimensional (0D) and one-dimensional (1D) nano-structures, which may bring new breakthroughs in the research field of nanotechnology. For instance, with the rise of energy storage industries, 2D nanostructures are considered to be promising candidates in lithium-ion batteries, because of their reduced lithium ion diffusion paths and large surface area allowing more lithium-ion intercalation.[10]

Among a large number of candidates for 2D nanomaterials, the IV-VI semiconductors which include GeS, GeSe, SnS and SnSe, etc. have become a hot research spot recently, because their bulk state could exhibit various electrical and optical properties suitable for numerous applications.[11] As one typical representative of these materials, SnSe has been viewed to have a wide range of meaningful applications (e.g. near-infrared optoelectronic devices, memory switching devices, solar cells, electrode material for rechargeable lithium-ion batteries, etc.).[12] In addition, compared to toxic lead, cadmium, or hydrargyrum-containing minerals, SnSe is also considered to be an environment-friendly material that could be used as more appropriate building blocks for semiconductor devices.[13]

Despite its own so many prominent advantages, so far, the progresses toward developing the potential of SnSe nanostructures have been still slow. Hence, the characteristics in the nano-scale of SnSe are almost to a large extent unknown. Only scattered reports have been presented, such as 0D nanocrystals,[14,15] 1D nanowires,[12,16] and 2D colloidal nanosheets.[17,18] Furthermore, obviously, all of these reports are focused on the so-called wet chemical synthetic approach. In general, these methods require complex procedures, harmful intermediate chemicals, and sometimes much longer reaction time. From this point of view, a different strategy should be needed for the simple growth of SnSe nanostructures. Among all the other nanomaterial synthesis techniques commonly used, vapour phase synthesis has been proved to be one of the most effective approaches, owing to its handle simplicity, reaction hypotoxicity, bottom-up growth characteristics to easily assemble less defects, and more homogeneous chemical composition products. For example, large-area, high-quality, and well-controlled graphene, layered h-BN and MoS_2 2D nanomaterials, etc., have been produced by exploiting the vapour medium, which are of great importance for practical applications.[19] Also, a noncatalytic vapour phase route has been reported for the growth of $SnSe_2$ nanoplates by Cao et al. and they reported mainly the effect of substrates to grow the nanoplates. However, their $SnSe_2$ nanoplates grew parallel to the substrates and the formation mechanism of the 2D nanoplate itself was not explored in detail based upon crystallography.[20]

In this paper we for the first time present a simple vapour growth approach for synthesizing high-density SnSe nanosheets on solid substrates without employing any catalysts. Since only

SnSe powder was used as a precursor instead of possible other toxic materials, such as $SnCl_2$, Se, or organometallic precursors, the synthesis process was much safer and easier to be operated. Also, SnSe nanosheets showed the substrate independent features that could grow quasi-vertically on several different kinds of substrates like Si, SiO_2, and fluorine-doped tin oxide (FTO) glass. Furthermore, the detail growth mechanism of SnSe nanosheets was proposed based upon in-depth study of the anisotropic crystal structure of SnSe and transmission electron microscopy (TEM) analysis results.

Experiment

SnSe nanosheets were synthesized in a conventional horizontal one-zone tube furnace by evaporating SnSe powder directly (see ESI, Scheme S1). As a typical procedure, SnSe powder (Sigma Aldrich, 99.995% purity) loaded in a graphite boat was located at the center of a quartz tube chamber (2.5 cm in diameter and 80 cm in length), which was inserted into the horizontal tube furnace (Lindberg/Blue M). Sometimes the empty tube was heated to 1000 °C before experiments to exclude any possibly existing impurities. Several pieces of Si wafers were cleaned by acetone, methanol, and DI water in order and they were placed one by one in the downstream of the carrier gas to collect the products. Before each experiment, the quartz tube was evacuated for ~25 min and then flushed with the carrier gas for 1 h to decrease the oxygen content in the chamber. And then the center temperature was increased to 660 °C at a heating rate of 40 °C/min and maintained at this temperature for 1 h. Because of the temperature gradient, nanosheets were found to grow preferentially at the position of ~16.5 cm away from the hot center region of the furnace, where the temperature was measured to be ~300 °C by a thermocouple. After the growth, the furnace was cooled down to room temperature. A mixture of H_2 (10 sccm) and Ar (140 sccm) was used as a protecting and a carrier gas, respectively during the whole process. From the view of facile fabrication of electronic nanodevices, besides Si wafer, SiO_2 and fluorine-doped tin oxide (FTO) glass were also used as other two kinds of solid substrates. The growth on SiO_2 and FTO followed the same procedures as that on Si.

Field emission scanning electron microscopy (FESEM; Hitachi S-4300, Tokyo, Japan) was used to examine the morphological features of nanosheets. Phase and structure analyses of samples were conducted by X-ray diffraction (XRD, Rigaku D/MAX-2500 V/PC, Tokyo, Japan, λ=1.5406 Å). The detailed investigation of the crystal structure, crystallinity, and growth orientations was carried out using the high-resolution transmission electron microscopy (HRTEM; FEI Tecnai G2 F30, 300 kV). Fast Fourier transform (FFT) pattern of the images was obtained to confirm the crystalline structures and the growth orientations checked by HRTEM. Energy dispersive X-ray spectroscopy (EDS) attached to HRTEM was performed at an accelerating voltage of 300 kV to identify specific elements. Ultraviolet-visible-near infrared (UV-Vis-NIR) spectroscopy (Shimadzu UV-3600) was also used to characterize the optical properties of nanosheets at room temperature.

Results and discussion

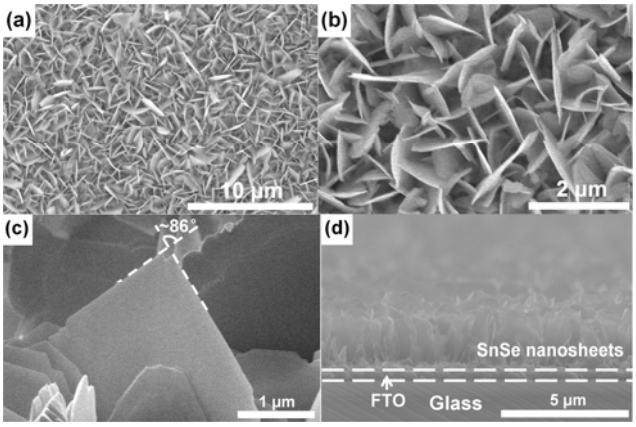

Fig. 1 (a) Low-magnification, (b) high-magnification FESEM images of SnSe nanosheets grown on Si, (c) typical morphology of a vertical nanosheet, and (d) cross-sectional view image of SnSe nanosheets on a FTO-glass substrate.

After the reaction, dark contrast could be observed at the substrate surface, indicating the successful deposition of SnSe nanosheets. Interestingly, the morphology of resulted nanosheets was nearly the same for all the three kinds of substrates. Compared to the nanodevices produced based on the transferred nanomaterials, this feature shows some considerable advantages, such as simplifying the processing procedure and enhancing material-substrate contact areas.[21] Fig. 1a and b are FESEM plan-view images of SnSe nanosheets taken at low and high magnifications, respectively. SnSe nanosheets completely covered the substrate with high-yield, and they are quasi-vertical to the substrate. They are touching each other to form a compact and randomly oriented morphology. This vertical growth is desirable, since more number of nanosheets can grow in the limited area of a substrate.[22-24] The thickness of nanosheets was estimated to be ~20−30 nm with the lateral dimension of ~2 μm. The typical morphology of a single nanosheet standing on the substrate is shown in Fig. 1c, indicating a square-like structure with a corner angle of ~86°. Furthermore, the FESEM cross-sectional view image (Fig. 1d) confirms the vertical growth of SnSe nanosheets on an FTO-glass substrate. The substrate independent characteristics of SnSe nanosheets were confirmed as shown in Fig. S1.

To analyze the phase and crystallinity of SnSe nanosheets, X-ray diffraction (XRD) was performed. Typical XRD patterns of SnSe nanosheets grown on a Si, FTO, and silica substrates are shown in Fig. 2, which indicates the highly crystalline nature of products. Possibly due to the disorder and random distribution characteristic of nanosheets on the substrates, the XRD patterns are similar to that of SnSe powder forms. Except the diffraction peaks detected from the sample holder (marked as "*", see the XRD pattern of holder inset of Fig. 2) and an unknown phase (▽), all the other diffraction peaks were identified to well correspond to the orthorhombic SnSe crystal structure with cell units of a = 11.50 Å, b = 4.15 Å, and c = 4.45 Å (JCPDS card No. 89-0232, Pnma 62).[18] However, the relative diffraction intensity of (011) planes was higher compared to that of other major diffractions such as (400) and (311). This implies that SnSe nanosheets have strong (011) component compared to SnSe powder samples. By exploiting Scherrer's formula, $D=0.89\ \lambda / \beta \cos\theta$ (D is the mean crystallite size, λ is the Cu Kα wavelength of 0.15406 nm, β is the

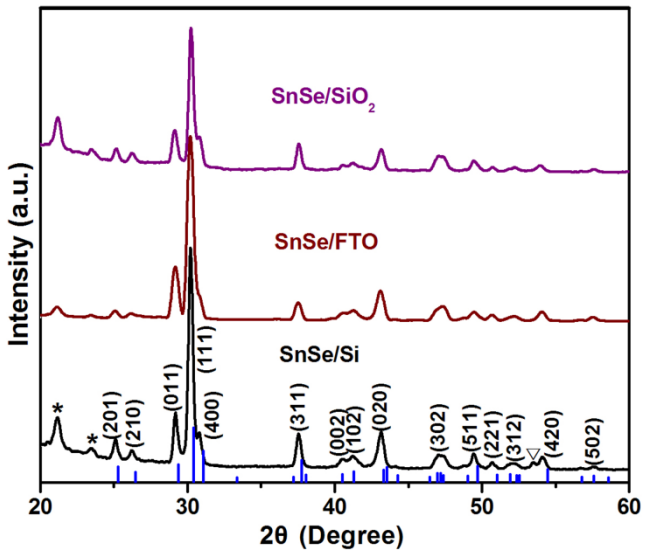

Fig. 2 XRD pattern of SnSe nanosheets grown on Si. FTO, and silica substrates. Here, "*" and "▽" denote diffractions from a sample holder and an unknown phase, respectively.

full-width at half maximum, and θ is the diffraction angle in degrees), the average crystallite size of (011) planes was determined to be ~22 nm. This value well corresponds to the thickness of SnSe nanosheets observed by SEM in Fig. 1.

In order to further elucidate the microstructure of obtained products, high-resolution transmission electron microscopy (HRTEM) investigation was conducted. Fig. 3a and b present the corresponding images of typical nanosheets with different magnifications. In Fig. 3a, the single crystallinity was observed from a SnSe nanosheet and its corner angle was measured as ~86°. Fig. 3b demonstrates that nanosheets are free of crystalline defects, such as stacking faults. Well-ordered lattice fringes and fast Fourier transform pattern (FFT, inset of Fig. 3b) could be obtained. Both of the lattice spacings along two directions are identically ~0.3 nm, and an intersection angles between them are ~86°. By considering the 2D crystal structure model (Fig. 3c) showing the atomic arrangement, lattice plane distances, and interatomic angles of the planes, the two atomic planes were identified as {011}. It should be noted here that through careful calculation by using standard lattice parameters, the intersection angles of {011} planes were determined to be 86°. The corner angels of the nanosheets shown in Fig. 1c and 3a exactly match to this theoretical value, respectively. Furthermore, the spot pattern of the FFT is proved to be {*0kl*} set reflections. Thus, all of these results confirm that SnSe nanosheets are bounded by {011} planes and they are orientated with the exposed plane normal

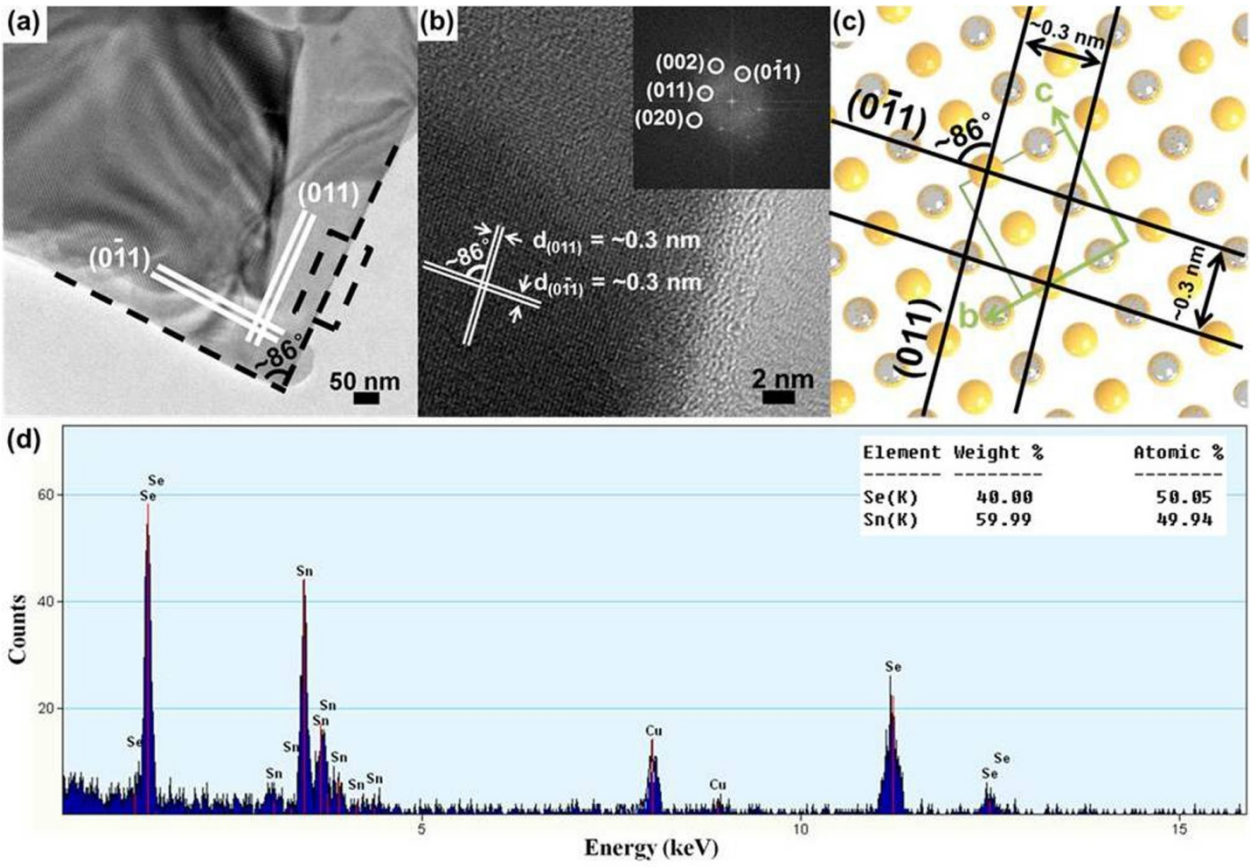

Fig. 3 (a) TEM image of typical SnSe nanosheets recorded at low magnification, (b) high magnification presenting the blown-up view of corresponding black box in (a), (c) 2D crystal structure model of orthorhombic SnSe showing the atomic arrangement, lattice spacing, and angles between {011} planes. The dotted line rectangle inside stands for the unit cell, and (d) corresponding EDS spectrum confirming the atomic ratio of Sn/Se to be ~1:1 (inset).

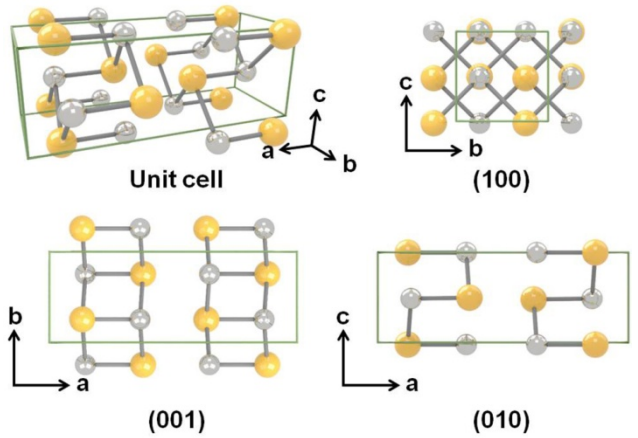

Scheme 1 3D crystal model of the orthorhombic SnSe unit cell and corresponding 2D views along the three coordinate directions.

along the [100] direction. In addition, the energy dispersive X-ray spectroscopy (EDS) spectrum of nanosheets (Fig. 3d) reveals that the atomic ratio of Sn:Se is ~1:1 (exact value is 49.94:50.05, inset of Fig. 3d), confirming their phase pure feature.

As a next step, we discuss in detail the growth mechanism of SnSe nanosheets synthesized in such physical vapour medium. Recently, the oriented attachment growth mechanism was used to account for the formation of colloidal SnSe nanosheets in which the initially formed SnSe nanoparticles might be driven by the dipole moment to be assembled into two dimensional nanostructures.[17,18] However, this mechanism is valid only for the wet-chemical method and it does not work for the present nanosheets. Also, there were no growth inhibitors suppressing the growth of certain specific atomic planes to lead to 2D nanosheet structures in the whole growth process. For instance, the adsorption of silicon or fluorine could suppress the (001) growth of TiO_2 to synthesize (001) TiO_2 nanosheets.[24,25] Thus, the growth mechanism of our nanosheets should be related to the crystal structure of itself. It is similar to ZnO nanorods that in general preferentially grow into the *c*-axis orientation due to the crystal structure anisotropy of the wurztite structure.[26] As is widely known, SnSe (similar to GeSe, GeS, and SnS) crystallizes in an orthorhombic layered crystal structure, having eight atoms in each unit cell. These atoms form two adjacent double layers that are perpendicular to the direction of the longest axis (*a*-axis in Scheme 1). Strong covalent bonds present within atomic layers, while weak van der Waals forces exist across atomic layers.[13,27] Typical 3D model of its unit cell and corresponding views along three coordinate directions are shown in Scheme 1.

We propose herein that the anisotropic atomic bonding nature of SnSe plays a crucial role in the formation of nanosheets. When Sn and Se atoms that are thermally decomposed from the source materials arrive at the substrate surface, nuclei could first form on the physically or chemically heterogeneous sites of the substrates (such as surface roughness or impurities, etc.) in a very short time. With continuously providing the precursor vapour, because of the significant difference between covalent bonding and van der Waals attraction, Sn and Se atoms could preferentially attach to the dangling bonds (covalent bonds) in the *b*- and *c*-axis directions. Thus, the crystal growth rate will be much faster in *b*- and *c*-axis orientations compared to the *a*-axis, leading to the formation of the 2D nanosheet morphology.

For the present SnSe crystal structure, the *a*-axis is the longest one among three axes. Thus, as described above, only weak van der Waals forces exist between {100} atomic layers perpendicular to the *a*-axis. Due to such characteristic, the attachment of atoms to {100} planes is limited, resulting in the slowest growth along the *a*-axis (i.e., [100] direction). Thus, {100} planes could become the exposed planes of final nanosheets.

Next, we analyze the evolution mechanism of the edge planes of SnSe nanosheets. From the FFT of the HRTEM shown in Fig. 3b, we could find two sets of lattice spots indicating possible edge planes of nanosheets. One set stands for {011} planes, and the other set indicates {020} and {002} planes. Known from the Law of Bravais, the growth rates of atomic planes with higher surface energy are usually much higher than those of planes with lower surface energy. Ultimately, the former ones will disappear, while the latter ones will remain in the final structures.[28] The surface energy, γ of an atomic plane could be defined as follows:[29]

$$\gamma = \frac{\Delta H\, N}{2\, A\, N_A} \qquad (1)$$

where ΔH is the bond energy (for the case of diatomic molecules), N is the number of dangling bonds, A is the surface area, and N_A is the Avogadro's number (6.02×10^{23} /mol). By referring to a relevant reference, the ΔH value of Sn–Se is 401.3 kJ/mol.[30] Scheme 2a, b, and c show 3D structure models of {001}, {010}, and {011} planes with dangling bonds, respectively. It could be observed that there are four dangling bonds on both the {001} and {010} planes (for {010} plane, half of the left four dangling bonds belong to it), which is one more than that on {011} planes having three dangling bonds. The surface areas of {001}, {010}, and {011} in a unit cell are calculated to be 47.73 Å^2, 51.18 Å^2, and 69.98 Å^2, respectively. Then, by exploiting Equation (1), the corresponding surface energy values of three planes are determined to be $\gamma_{(001)} = 2.80$ J/m^2, $\gamma_{(010)} = 2.61$ J/m^2, and $\gamma_{(011)} = 1.43$ J/m^2, i.e., {011} planes have the lowest surface energy among the three planes. Therefore, for our SnSe nanosheets, {011} atomic planes could remain to serve as the exposed edge facets in the final morphology.

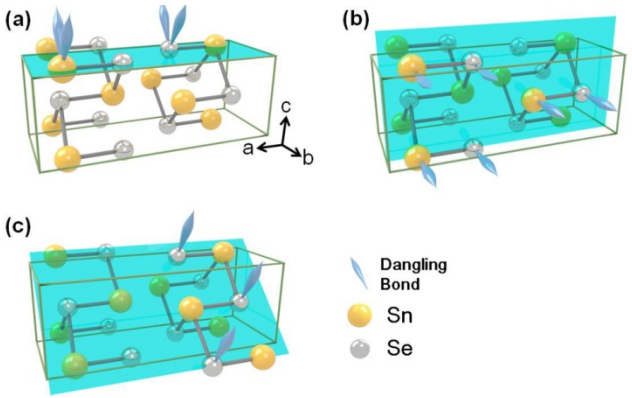

Scheme 2 3D crystal model of the orthorhombic SnSe showing (a) (001), (b) (010), and (c) (011) planes with dangling bonds.

Cite this: DOI: 10.1039/c0xx00000x

www.rsc.org/xxxxxx

ARTICLE TYPE

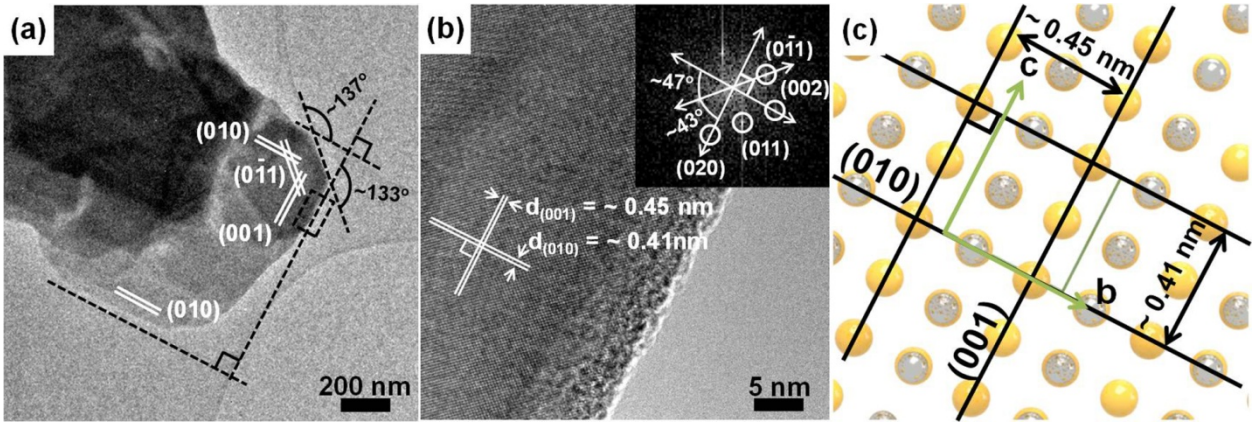

Fig. 4 (a) A TEM image of a SnSe nanosheet in the intermediate stage recorded at low magnification, (b) a high-magnification TEM image illustrating the blown-up view of corresponding black box in (a) (inset is the corresponding FFT pattern), and (c) 2D crystal structure model showing the atomic arrangement, lattice spacings, and angles between {001} and {010} planes. The rectangle inside represents the unit cell.

However, it is important to note here that once the furnace heating for the nanosheet synthesis ends, the growth of nanosheets will be also immediately terminated. Thus, besides the majority of nanosheets in the final stage, there should be some products staying in the intermediate stage probably due to the late nucleation. Fig. 4 shows TEM images of a nanosheet that is much smaller than that in Fig. 3a. In Fig. 4b, the lattice spacings of ~0.45 and ~0.41 nm combined with the intersection angle of 90° prove the edge planes (except the corner) to be {001} and {010}, based upon the 2D atomic arrangement model (Fig. 4c). As shown in Fig 4a, the angle between {010} and the corner facet was measured to be ~137° and that between {001} and the corner

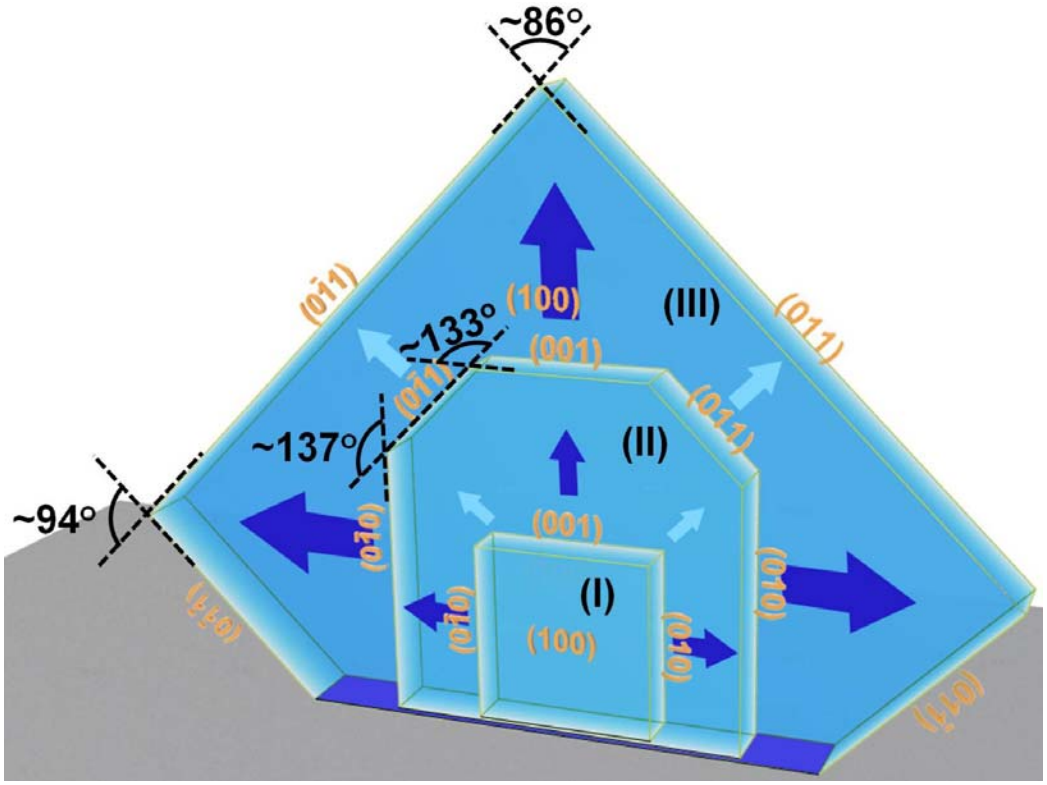

Scheme 3 A proposed growth model indicates the edge plane evolution of a SnSe nanosheet. Here, I, II, and III denote the initial, intermediate, and final stage of crystal growth, respectively and the size difference in arrows implies the difference in the growth rate of each atomic plane.

Cite this: DOI: 10.1039/c0xx00000x

www.rsc.org/xxxxxx

ARTICLE TYPE

angles of ~43° between {010} and {011} and ~47° between {001} and {011} as presented in the FFT (inset of Fig. 4b). Thus, the corner facets are proved to be {011} atomic planes. Therefore, it is evidenced that there indeed exists an intermediate stage for nanosheets in which {001} and {010} planes co-exist with {011} planes to comprise of the edge planes of SnSe nanosheets.

Based on all the above analyses for SnSe nanosheets, the evolution process of their edge planes could be described as follows, and the overall growth mechanism is depicted in Scheme 3. With Sn and Se atoms rapidly binding to dangling bonds at the surface of a SnSe nucleus, a small nanosheet having three edge planes could form, as denoted by Phase I. On the other hand, due to the lower surface energy, the growth rate of {011} planes could be so slow that they hardly appear in the early stage nanosheet morphology. Thus, in the initial stage a small nanosheet will firstly form a rectangular-like morphology bounded by {001} and {010} planes because of their faster growth rate (i.e. higher surface energy). The reason that the basal planes of SnSe nanosheets are {001} could be that {001} planes have the highest surface energy in a SnSe crystal. Since as shown in Fig. S1, the growth of SnSe nanosheets seems not to be affected by the substrates, they could grow preferentially along the high surface energy orientations. Then, as time goes on (Phase II), since the growth rates of {001} and {010} planes are high, while that of {011} planes is low, {011} planes start to appear as exposed edge planes at the corner of the nanosheets with corner angles calculated to be ~133° (or ~47°) and 137° (or ~43°). In the final stage (Phase III) only {011} planes will be left behind to become the final edge planes of SnSe nanosheets and to maintain the whole crystal with a minimum surface energy. This result is in good agreement with the XRD data showing higher (011) peak intensity compared to the JCPDS standard, as shown in Fig. 2. Although {011} planes intrinsically have low-intensity XRD diffraction, they show increased intensity, since they are top edge planes of vertically grown SnSe nanosheets. On the other hand, although {100} or {400} planes intrinsically have relatively high-intensity diffraction and they are almost all the exposed surface in our SnSe nanosheets, they show low diffraction intensity, since they are normal to the substrate and their thickness is only ~20–30 nm.

The light absorption behavior of SnSe nanosheets grown on a SiO_2 substrate was investigated using UV/Vis/NIR absorbance spectroscopy, which is shown in Fig. 5. SnSe nanosheets showed broad light absorption from near infra-red (NIR) to visible range with absorption onset of ~1,190 nm. To obtain the direct energy band gap of SnSe nanosheets, Kubelka-Munk transformation was conducted. The absorption spectrum was converted by following equation for the near-edge absorption:[31]

$$(ahv)^{n} = K(hv - E_g) \quad (2)$$

where K is a material constant, α is the absorption coefficient, hv is the photon energy, and n is 2 for a direct band gap semiconductor. Due to a linear relation between the absorbance (A) and the absorption coefficient (α), the extrapolation of the transformed $(A \cdot hv)^2$ vs. photon energy plot demonstrates a direct energy band gap (E_g) of 1.1 eV for our SnSe nanosheets (inset ofFig. 5), which is well consistent with the former reports dealing with SnSe nanomaterials.[18,32] The IR and visible light absorption behavior of SnSe nanosheets well demonstrates the strong potential to be used for photovoltaic applications.[33,34] The 2D nanosheet structures vertically grown at the substrates with high density could be highly beneficial for the fabrication of dye-sensitized solar cells (DSSCs) and hybrid solar cells since organic dyes or conducting polymers can be more easily overcoated to the nanosheet surface compared to other nanostructures.

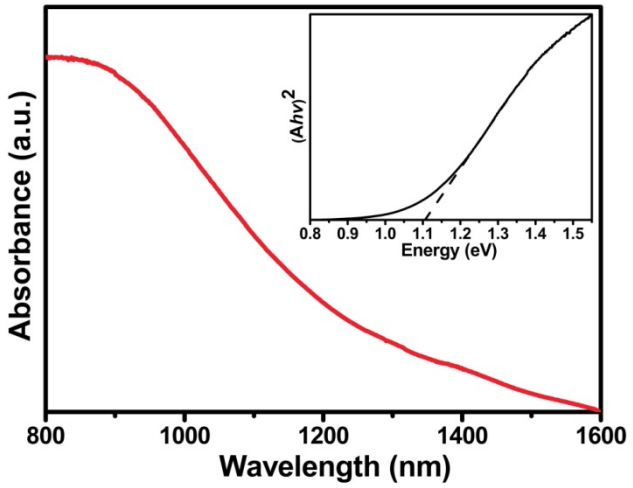

Fig. 5 UV-VIS-NIR absorbance spectrum of SnSe nanosheets and the corresponding $(A \cdot hv)^2$ vs. photon energy plot (inset) for determining the direct energy band gap.

Conclusions

To conclude, high density and quasi-vertical two-dimensional SnSe nanosheets with the thickness of ~20–30 nm and the lateral size of several micrometers have been successfully synthesized via a catalyst-free vapour phase synthesis method. They showed the substrate independent growth on Si, SiO_2, and FTO glass. The crystal growth mechanism was proposed for SnSe nanosheets through in-depth analyses on the crystal structure of orthorhombic SnSe and corresponding experimental results. The anisotropic atomic bonding nature and the surface energy difference in each atomic plane played a decisive role in the growth of 2D SnSe nanosheets and in the formation of the edge planes. We expect that the mechanism we proposed here could be extended to the interpretation of other 2D nanosheets grown by vapour phase synthesis process. Moreover, this mechanism could be utilized to grow crystallographically anisotropic materials into new 2D nanosheet structures. The energy band gap of SnSe nanosheets was determined to be ~1.1 eV, corresponding to 1,127 nm that is in the near infra-red (NIR) region. Thus, they can

absorb considerable portion of the solar spectrum mostly comprised of visible and IR lights. Therefore, combining this light absorption property with their substrate independent characteristics, it is expected that our SnSe nanosheets could be used as building blocks for high performance and low-cost solar cells.

Acknowledgements

This work was supported by the National Research Foundation (NRF) of Korea grants funded by Korean government (2013R1A1A2072509). The authors thank Dr. H.-S. Baik of Korea Basic Science Institute (KBSI; Seoul, Republic of Korea) for his kind support for TEM works.

Notes

Department of Materials Science and Engineering, Korea University, Seoul 136-713, South Korea. Fax: +82 2 928 3584, Tel: +82 2 3290 3286, E-mail: ymsung@korea.ac.kr

† Electronic Supplementary Information (ESI) available: Experimental setup (Scheme S1), SEM images of SnSe nanosheets grown on different substrates (Figure S1) and XRD patterns of SnSe nanosheets grown on SiO_2 and FTO glass substrates (Figure S2). See DOI: 10.1039/b000000x/

‡ The two authors equally contributed to this work as co-first authors.

References

1 K. S. Novoselov, Z. Jiang, Y. Zhang, S. V. Morozov, H. L. Stormer, U. Zeitler, J. C. Maan, G. S. Boebinger, P. Kim and A. K. Geim, *Science*, 2007, **315**, 1379.
2 A. A. Balandin, S. Ghosh, W. Z. Bao, I. Calizo, D. Teweldebrhan and F. Miao, C. N. Lau, *Nano Lett.*, 2008, **8**, 902.
3 R. R. Nair, P. Blake, A. N. Grigorenko, K. S. Novoselov, T. J. Booth, T. Stauber, N. M. R. Peres and A. K. Geim, *Science*, 2008, **320**, 1308.
4 Z. Y. Wang, B. B. Huang, Y. Dai, Y. Y. Liu, X. Y. Zhang, X. Y. Qin, J. P. Wang, Z. K. Zheng and H. F. Cheng, *CrystEngComm*, 2012, **14**, 1687.
5 M. M. Atabaki and R. Kovacevic, *Electron. Mater. Lett.*, 2013, **9**, 133.
6 Y. Zhao, Y. Huang, Q. F. Wang, X. Y. Wang, M. Zong, H. W. Wu, and W. Zhang, *Electron. Mater. Lett.*, 2013, **9**, 683.
7 M. Du, Y. Z. Wu and X. P. Hao, *CrystEngComm*, 2013, **15**, 1782.
8 M. Chhowalla, H. S. Shin, G. Eda, L.-J. Li, K. P. Loh and H. Zhang, *Nat. Chem.*, 2013, **5**, 263.
9 J. S. Chen and X. W. Lou, *Mater. Today*, 2012, **15**, 246.
10 J. H. Liu and X.-W. Liu, *Adv. Mater.*, 2012, **24**, 4097.
11 M. S. Xu, T. Liang, M. M. Shi, and H. Z. Chen, *Chem. Rev.*, 2013, **113**, 3766.
12 S. Liu, X. Y. Guo, M. R. Li, W.-H. Zhang, X. Y. Liu and C. Li, *Angew. Chem. Int. Ed.*, 2011, **50**, 12050.
13 P. D. Antunez, J. J. Buckley and R. L. Brutchey, *Nanoscale*, 2011, **3**, 2399.
14 M. A. Franzman, C. W. Schlenker, M. E. Thompson and R. L. Brutchey, *J. Am. Chem. Soc.*, 2010, **132**, 4060.
15 W. J. Baumgardner, J. J. Choi, Y. F. Lim and T. Hanrath, *J. Am. Chem. Soc.*, 2010, **132**, 9519.
16 G. Z. Shen, D. Chen, X. A. Jiang, K. B. Tang, Y. K. Lui and Y. T. Qian, *Chem. Lett.*, 2003, **32**, 426.
17 D. D. Vaughn18 II, S.-I. In and R. E. Schaak, *ACS Nano*, 2011, **5**, 8852.
18 L. Li, Z. Chen, Y. Hu, X. W. Wang, T. Zhang, W. Chen and Q. B. Wang, *J. Am. Chem. Soc.*, 2013, **135**, 1213.
19 X. F. Song, J. L. Hu and H. B. Zeng, *J. Mater. Chem. C*, 2013, **1**, 2952.
20 L. Huang, Y. Yu, C. Li and L. Cao, *J. Phys. Chem. C*, 2013, **117**, 6469.
21 J. Jiang, Y. Y. Li, J. P. Liu and X. T. Huang, *Nanoscale*, 2011, **3**, 45.
22 Z. Bo, Y. Yang, J. H. Chen, K. H. Yu, J. H. Yan and K. F. Cen, *Nanoscale*, 2013, **5**, 5180.
23 Q. H. Mu, Q. H. Zhang, H. Z. Wang and Y. G. Li, *J. Mater. Chem.*, 2012, **22**, 16851.
24 W.-J. Lee and Y.-M. Sung, *Cryst. Growth Des.*, 2012, **12**, 5792.
25 X. G. Han, Q. Kuang, M. S. Jin, Z. X. Xie and L. S. Zheng, *J. Am. Chem. Soc.*, 2009, **131**, 3152.
26 J.-Y. Chang, T. G. Kim and Y.-M. Sung, *Nanotechnol.*, 2011, **22**, 425708.
27 L. Makinistian and E. A. Albanesi, *Phys. Status Solidi B*, 2009, **246**, 183.
28 J. D. H. Donnay and D. Harker, *Am. Mineral.*, 1937, **22**, 446.
29 M. W. Barsoum, *Fundamentals of Ceramics*, ed. R. Gibala, M. Tirrell, and C. A. Wert, McGraw-Hill, New York, Interational, 2000, ch. 4, pp. 110.
30 J. G. Speight, *Lange's Handbook of Chemistry*, McGraw-Hill, New York, 16th edn., 2005, ch. 1, pp. 1.170.
31 A. Hagfeldt and M. Gratzel, *Chem. Rev.*, 1995, **95**, 49.
32 N. R. Mathews, *Sol. Energy*, 2012, **86**, 1010.
33 H. M. Jia, W. W. He, X. W. Chen, Y. Lei and Z. Zheng, *J. Mater. Chem.*, 2011, **21**, 12824.
34 Y. Lei, H. M. Jia, W. W. He, Y. G. Zhang, L. W. Mi, H. W. Hou, G. S. Zhu, and Z. Zheng, *J. Am. Chem. Soc.*, 2012, **134**, 17392.